Interfaces and surfaces of solids with polar terminations

Ilya Elfimov

Stewart Blusson Quantum Matter Institute
THE UNIVERSITY OF BRITISH COLUMBIA

ampel

UBC

Classification of Ionic Crystals Surfaces

Type 3 : planes are charged and there is dipole in repeat unit

(111) surface of simple oxides with rock salt crystal structure EuO, NiO, MnO ...

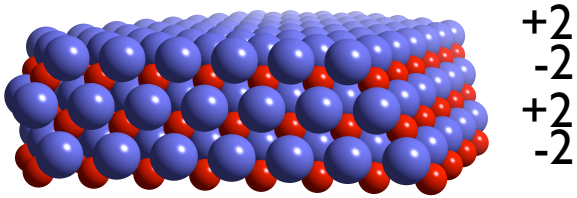

(001) surface of trivalent perovskites $LaAlO_3$, $LaMnO_3$ ...

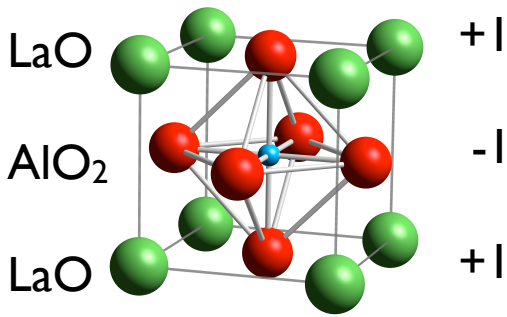

$BaFe_2As_2$

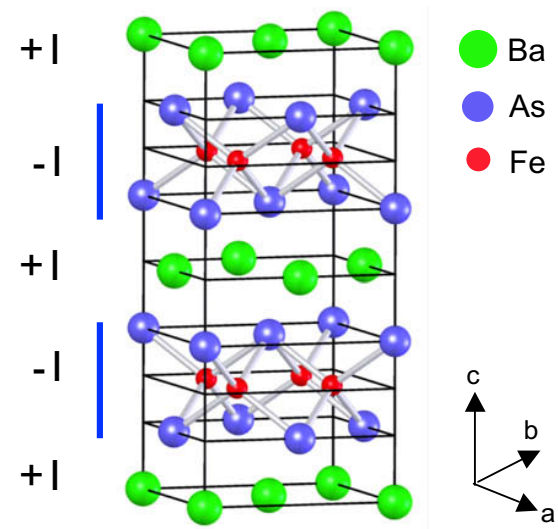

YBCO: Taking advantage of electronic reconstruction.

Type 3 surfaces are unstable. They have to reconstruct.

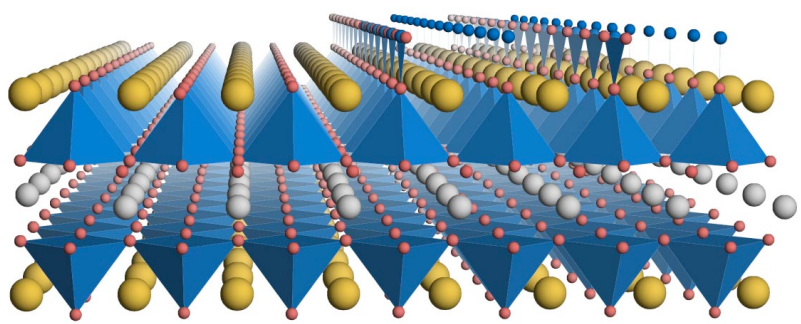

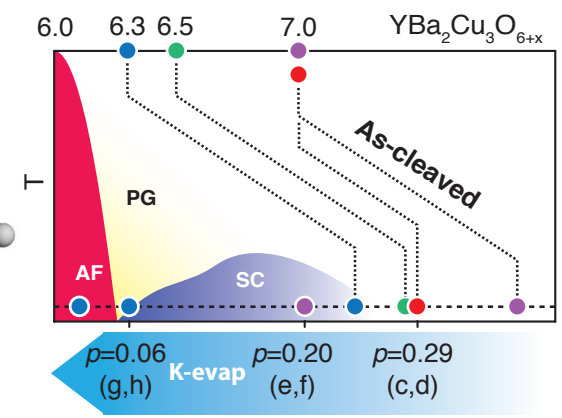

David Fournier et al, accepted in Nature Physics

P.W. Tasker, J. Phys. C **12**, 4977 (1979)

Classification of Ionic Crystals Surfaces

Type 2 : planes are charged but there is no dipole in repeat unit

TiS_2

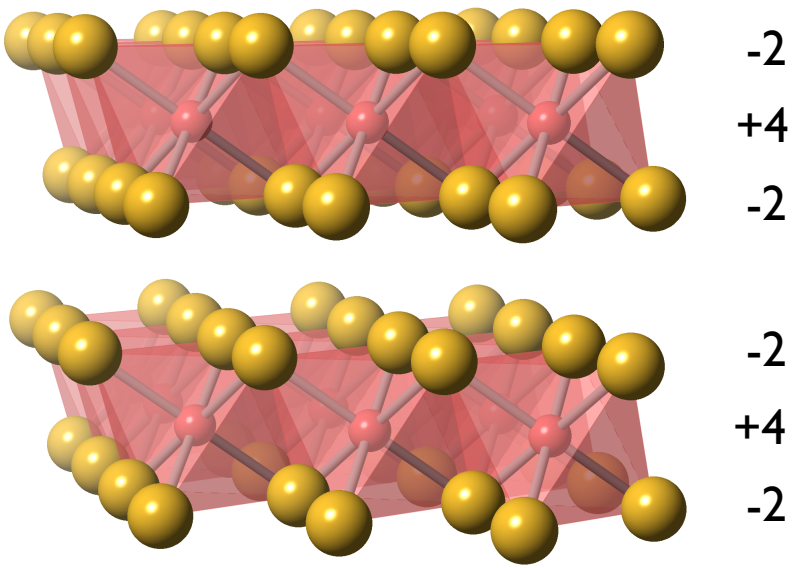

LiFeAs

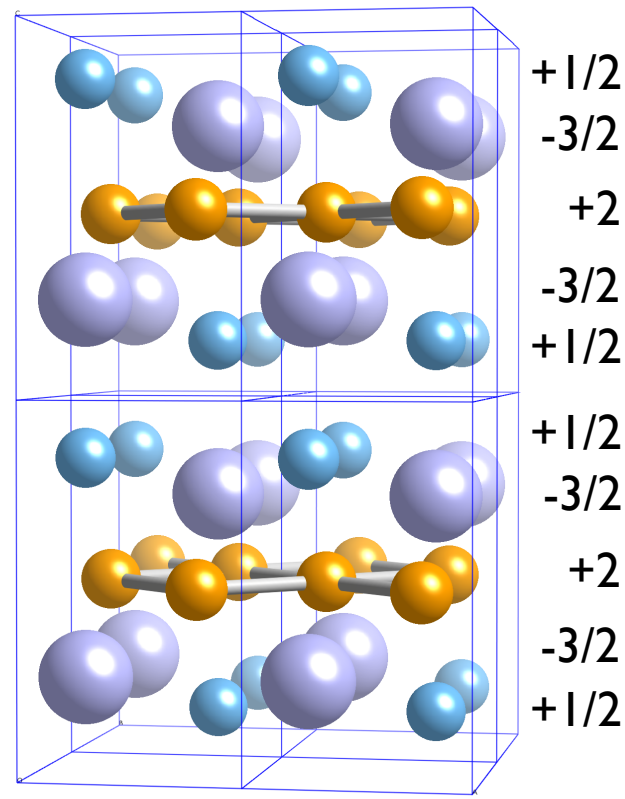

BISCO, La_2CuO_4 ...

P.W. Tasker, J. Phys. C **12**, 4977 (1979)

Classification of Ionic Crystals Surfaces

Type 1 : all planes are charge neutral

(001) surface of tetravalent perovskites
$SrTiO_3$ ...

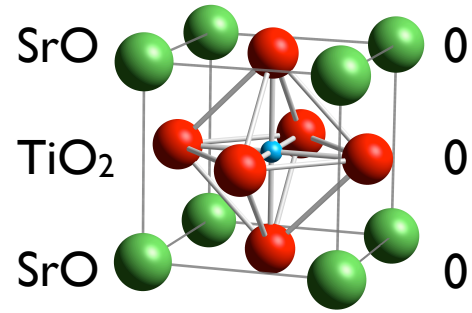

(001) and (110) surface of simple oxides with rock salt crystal structure
MgO, NiO, EuO, MnO ...

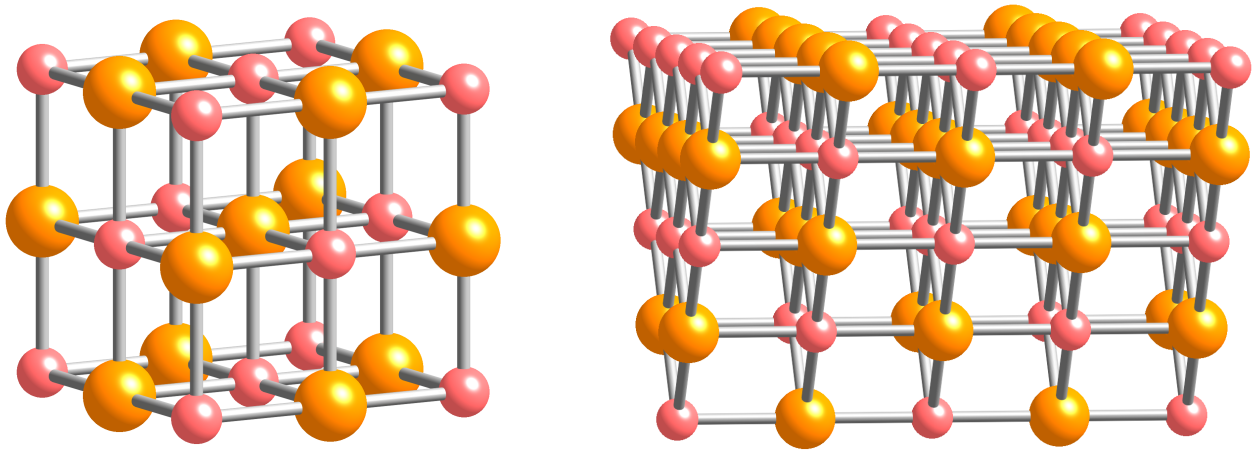

P.W. Tasker, J. Phys. C **12**, 4977 (1979)

2D electron gas at LAO/STO interface

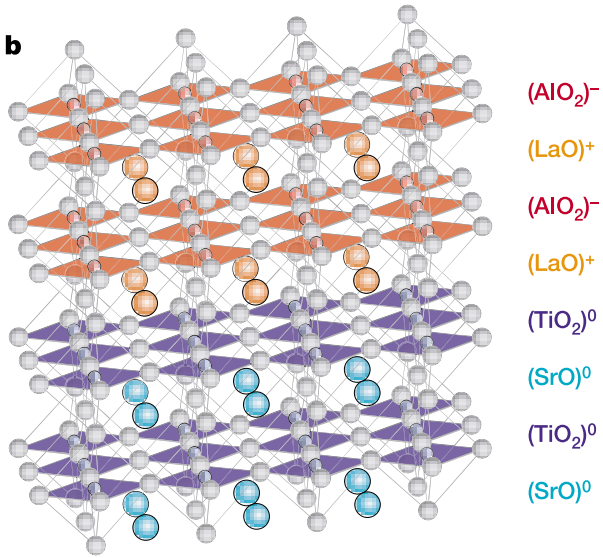

A. Ohtomo and H.Y. Hwang *Nature* **427**, 423 (2004)

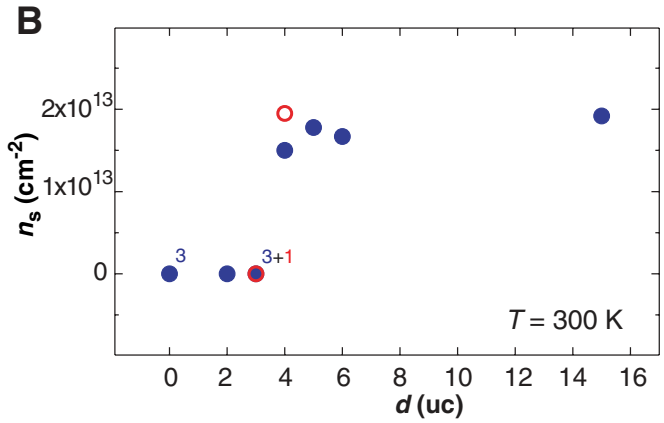

S. Thiel, et al. *Science* **313**, 1942-1945 (2006)

- Only LaO-TiO_2 (i.e. n-type) interface is conducting
- Critical thickness
- Contradicting reports of carrier density often non-consistent with theoretical predictions $2x10^{13}$ (Hall constant) $1.1x10^{14}$ (core level XPS) vs $3.4x10^{14}$ cm^{-2} (formal ionic charges). Except materials with common cat ion ($GdTiO_3$/$SrTiO_3$).
- High sensitivity to growth condition. Higher Oxygen pressure seems to produce insulating samples.

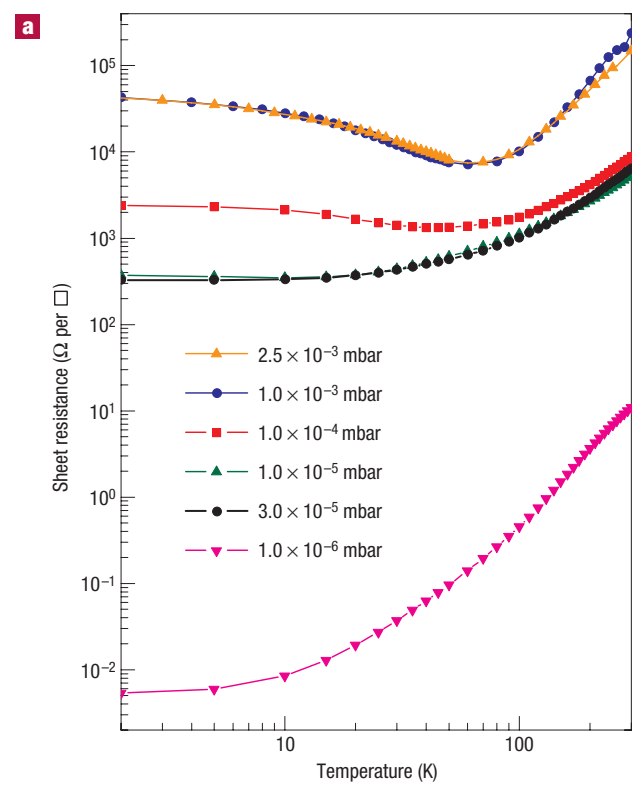

Sing, M. et al. *Phys Rev Lett* **102**, 176805 (2009)

A. Brinkman, et al. *Nat Mater* **6**, 493-496 (2007)

Oxide Nanoelectronics on Demand

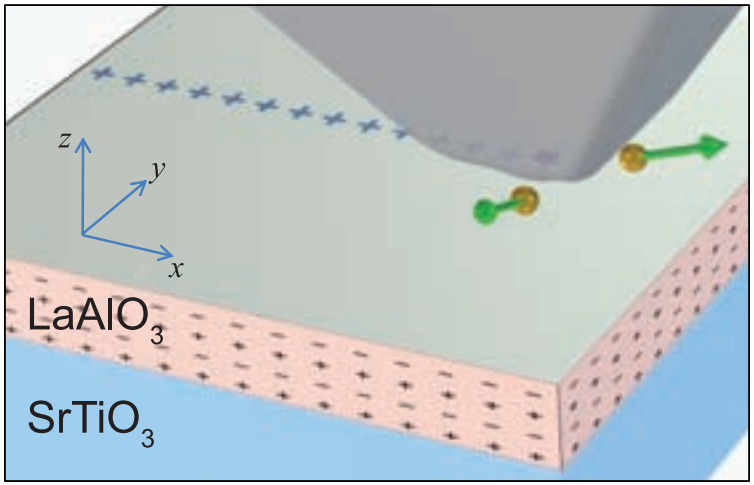

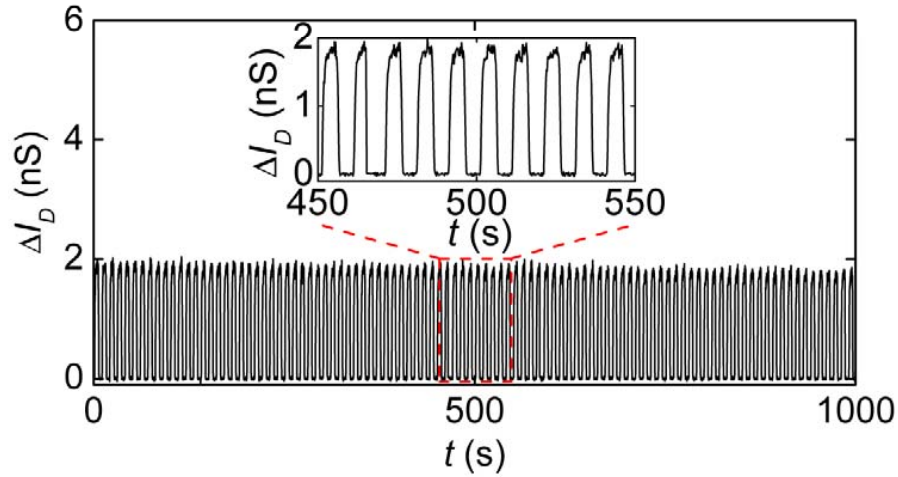

Repeated cutting and restoring of a 12 nm nanowire using Vtip = +/- 10V

Fig. 2. SketchFET device. (**A**) Schematic diagram of SketchFET structure. S, source electrode; D, drain electrode; G, gate electrode. (**B**) *I-V* characteristic between source and drain for different gate biases $V_{GD} = -4$ V, -2 V, 0 V, 2 V, and 4 V. (**C**) Intensity plot of I_D (V_{SD}, V_{GD}).

A

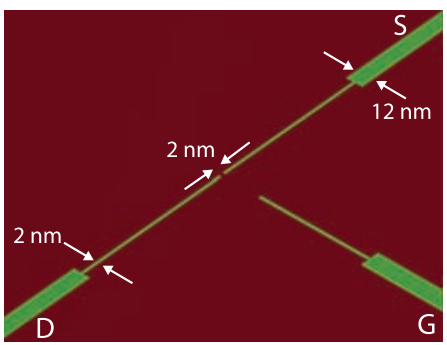

Possible explanations

1) Local structural modifications
2) Vacancies
3) H_2O

...

C. Cen et al, Science 323, 1026 (2009)

Writing with water

Charge writing on bare (001) LAO and (001) STO substrates

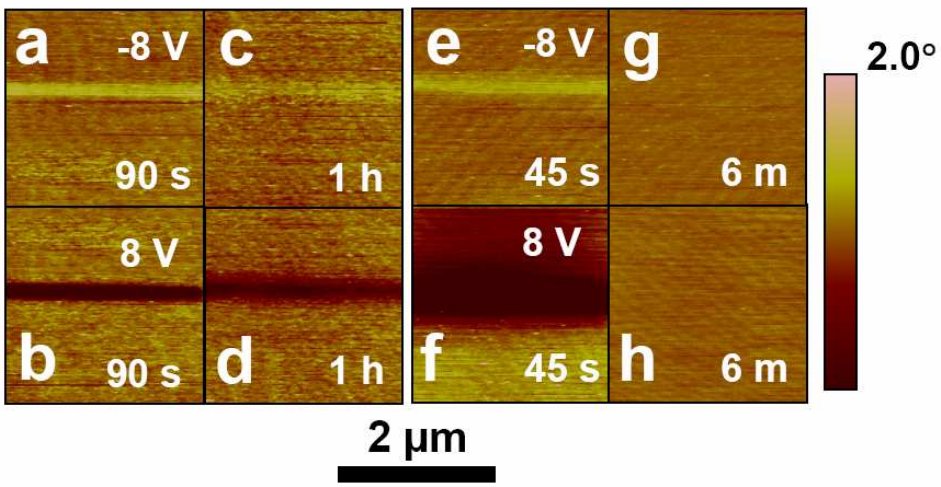

FIGURE S1. Charge writing on bare (001) LAO and (001) STO substrates. Written features on LAO with (a), -8 V (b), +8 V acquired after 90 seconds. (c, d) The same areas as (a) and (b), respectively, acquired after 1 hour. Features on STO, written with (e) -8 V (f) +8 V acquired after 45 seconds. (g, h) The same areas as in (e) and (f), respectively, acquired after 6 minutes. All images were acquired with V_{read} = -2 V.

Yanwu Xie et al, Nano Letters 10, 2588 (2010)

A straightforward test of the water cycle mechanism outlined above replaces atmospheric conditions with gas environments that lack H_2O. Figure 2 shows the results of a number of writing experiments performed using dry air [Fig. 2(a)], helium gas [Fig. 2(b)], and dry nitrogen [Fig. 2(c)] under pressures ranging from 10^{-2}–10^{2} Torr. Nanowires were not formed under any of these conditions. To verify that the sample was not adversely affected during these experiments, the sample was subsequently exposed to air (28% relative humidity) and a nanowire was written with ~120 nS conductance [Fig. 2(d)]. The nanowire was then erased and the AFM was evacuated to base pressure (1.8×10^{-5} Torr). Under vacuum conditions, it was again not possible to create conducting nanostructures.

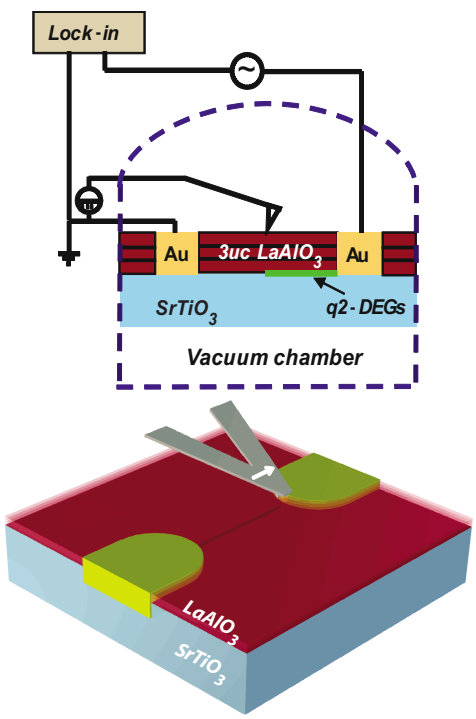

Feng Bi et al, APL 97, 173110 (2010)

Heterostructures with common cation ($GdTiO_3/SrTiO_3$)

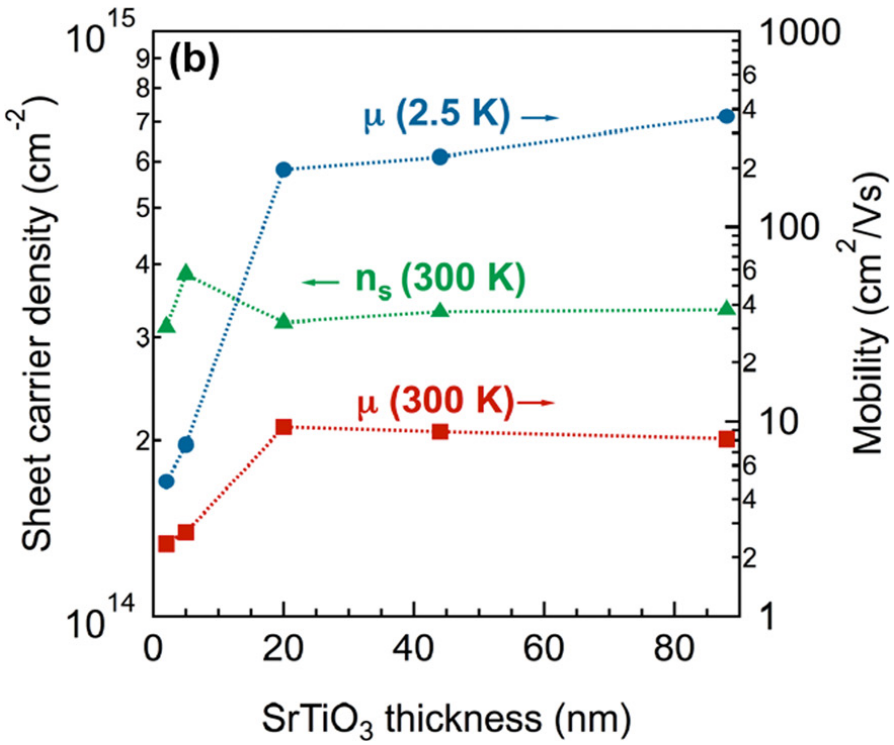

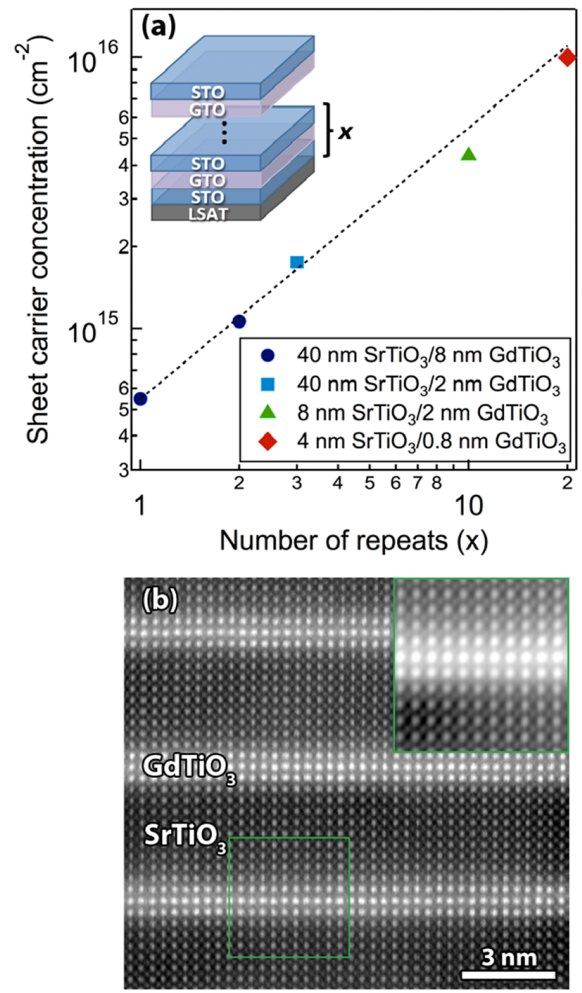

FIG. 2. (Color online) (a) Room temperature sheet carrier concentrations of $SrTiO_3/GdTiO_3/SrTiO_3$ multilayers as a function of multilayer repeats (x). The dashed line indicates the expected sheet carrier concentration scaling with number of repeats as calculated from the $x = 1$ sample. (b) High-angle annular dark-field scanning transmission electron microscopy image of the $x = 20$ multilayer.

P. Moetakef, et al. *Appl. Phys. Lett.* **99**, 232116 (2011)

Origin of the 2D electron gas

Band banding:

K. Yoshimatsu et al., Phys. Rev. Lett. 101, 026802 (2008)

Oxygen vacancies in STO:

W. Siemons et al., Phys. Rev. Lett. 98, 196802 (2007)
G. Herranz et al., Phys. Rev. Lett. 98, 216803 (2007)
A. Kalabukhov et al., Phys. Rev. B 75, 121404(R) (2007)

Cation intermixing :

P. R. Willmott et al., Phys. Rev. Lett. 99, 155502 (2007)
A. S. Kalabukhov et al., Phys. Rev. Lett. 103, 146101 (2009)

Electronic reconstruction.

A. Ohtomo and H.Y. Hwang Nature **427**, 423 (2004)

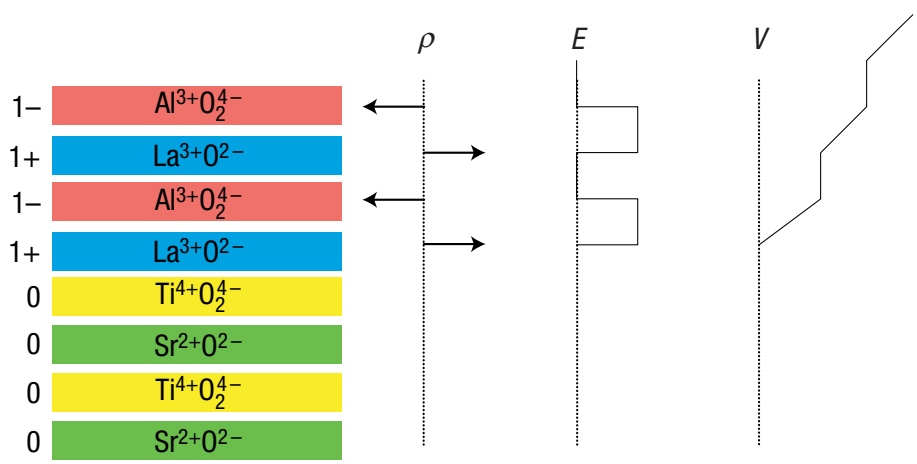

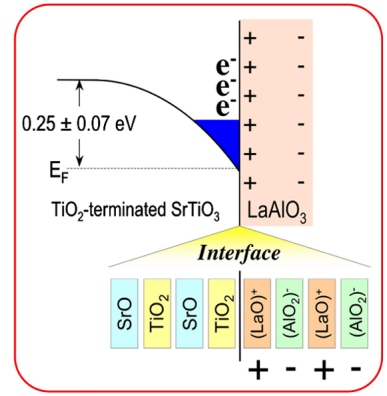

Electrons are generated by the Oxygen vacancies in the bulk STO

Bulk $Sr_{1-x}La_xTiO_3$ is metallic

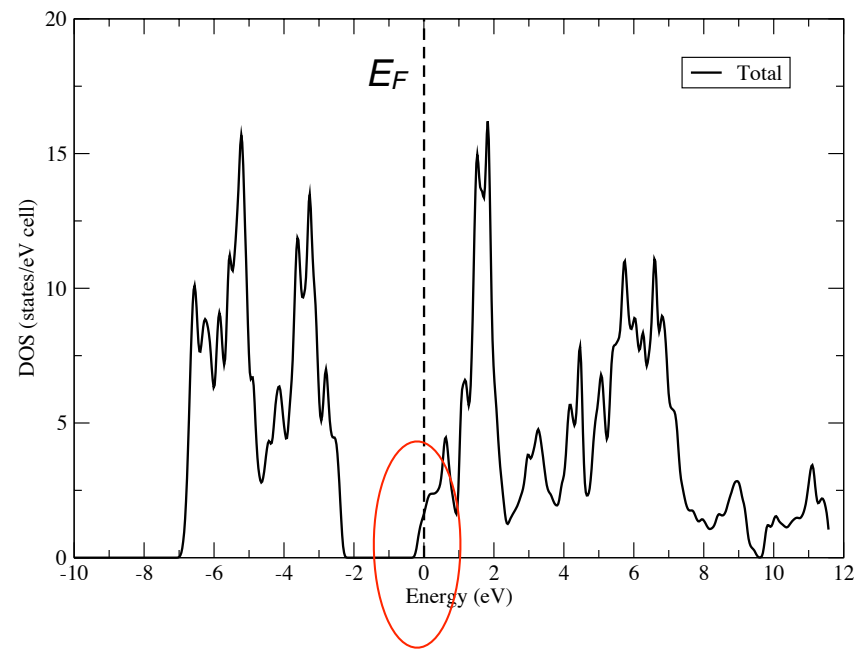

Charge compensating electrons

Origin of potential divergence

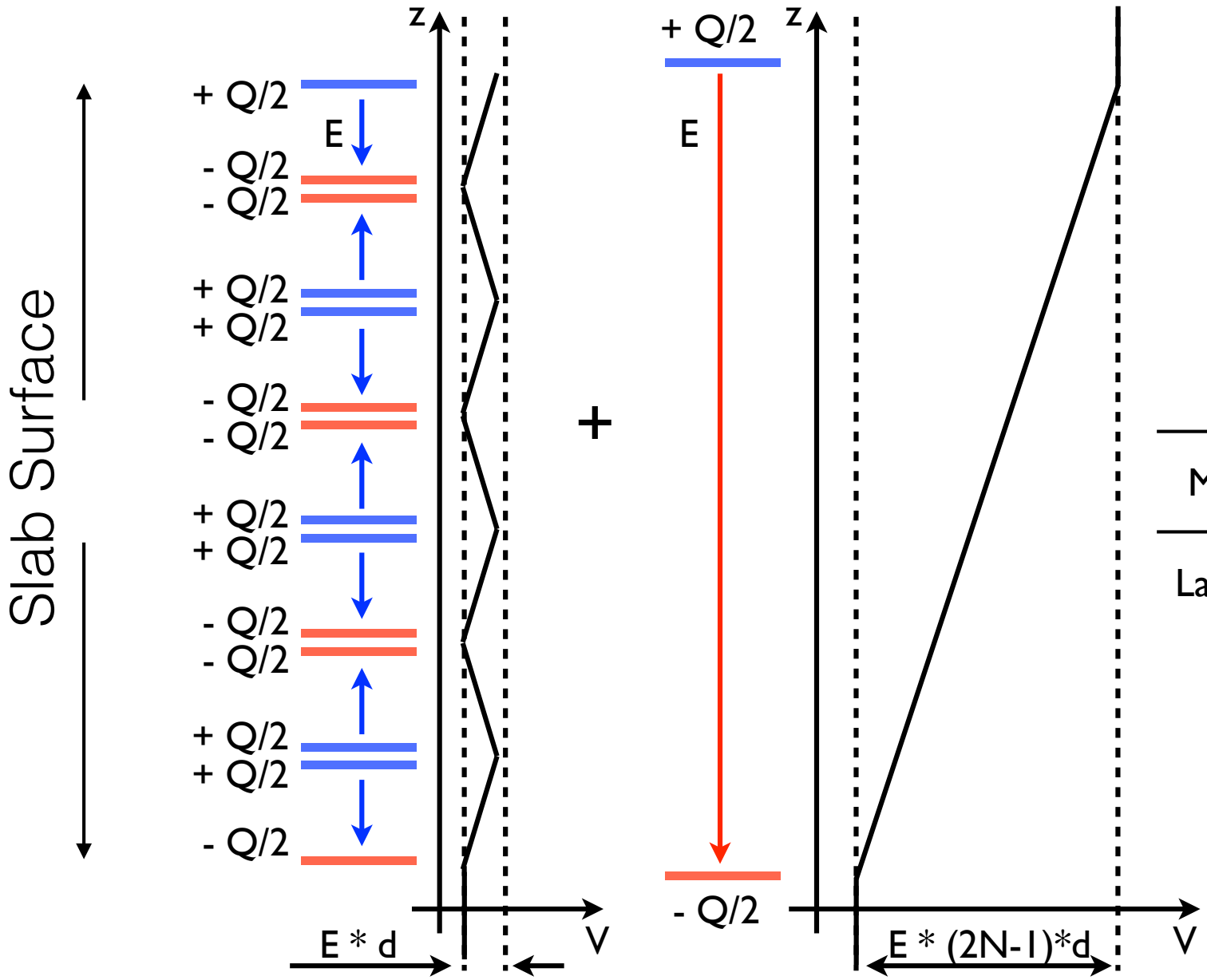

In $LaAlO_3$
$Q/2=3.4\times10^{14}$ cm^{-2}
or 0.5e per AlO_2

	$V_{res}(V)$
MgO (111)	1002
$LaAlO_3$ (001)	418

Films are 18 bilayers thick
(4.3 nm MgO and 6.6 nm LAO)

Solution to polar catastrophe

a) charged surface vacancies
b) adatoms / surfactants
c) electronic reconstruction
charge transfer, dangling bonds, valence change etc

Vacancies or adions (K+, OH-, I-)

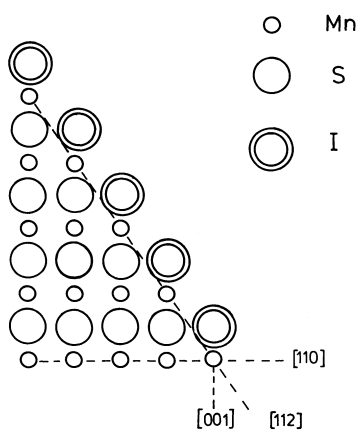

Fig. 2. The rocksalt structure of α-MnS projected on the (110) plane; the (111) surface consists of a layer of iodine ions.

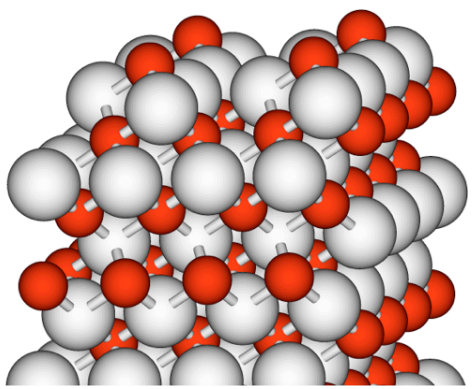

Octopolar reconstruction of (111) surface of materials with rock salt structure

Electronic reconstruction

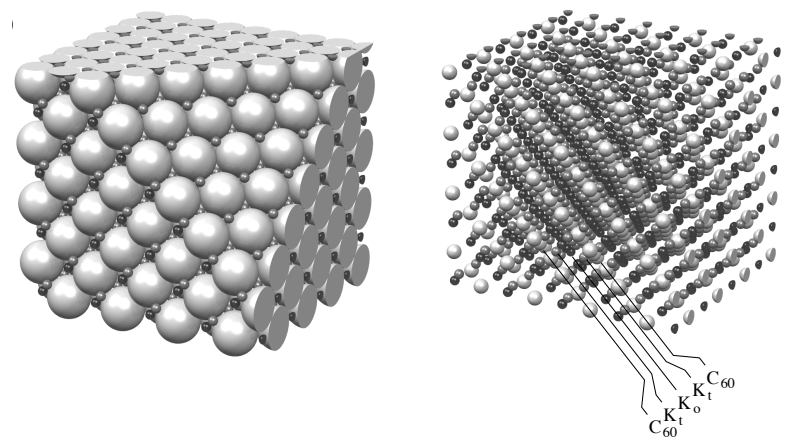

K_3C_{60}: R. Hesper et al., PRB **62**, 16046 (2000)
$LaAlO_3$ /$SrTiO_3$ interfaces: A. Ohtomo and H.Y. Hwang Nature **427**, 423 (2004)

K-deposition: M.A. Hossain et al., Nat. Phys. 4, 527 (2008)
OH- NiO (111): D. Cappus et al., Surf. Sci. 337, 268 (1995)
I- MnS (111): H.H. Heikens et al., Jap. J. Appl. Phys. suppl 19-3, 399 (1980)
Ba vacancies on $BaFe_2As_2$ surface: Y. Yin et al., Phys. Rev. Lett. 102, 97002 (2009)

Electronic reconstruction of SmB_6 (001) surface

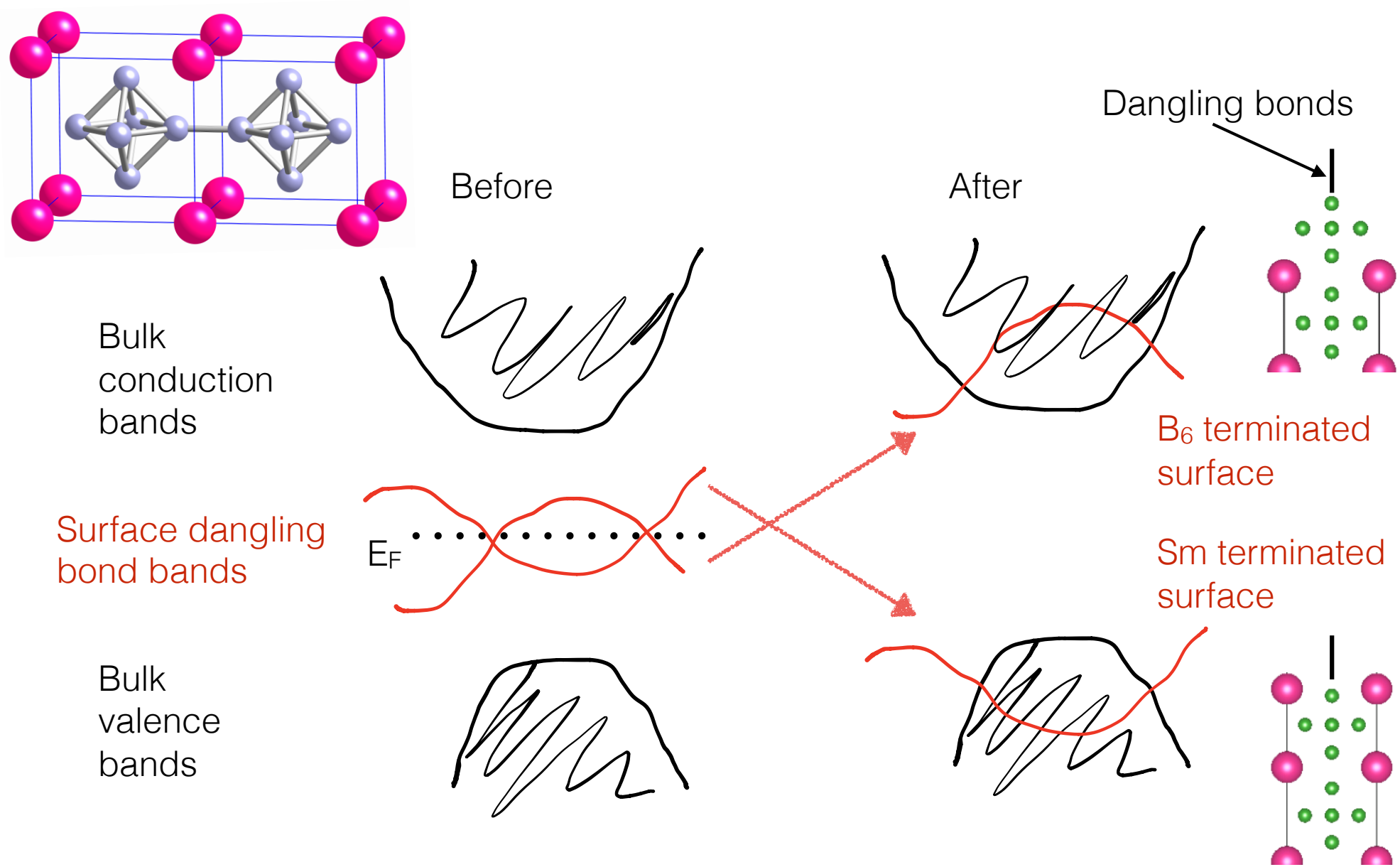

Z.-H. Zhu, et al. *Phys. Rev. Lett.* **111**, (2013)

Boron surface states: ARPES and DFT

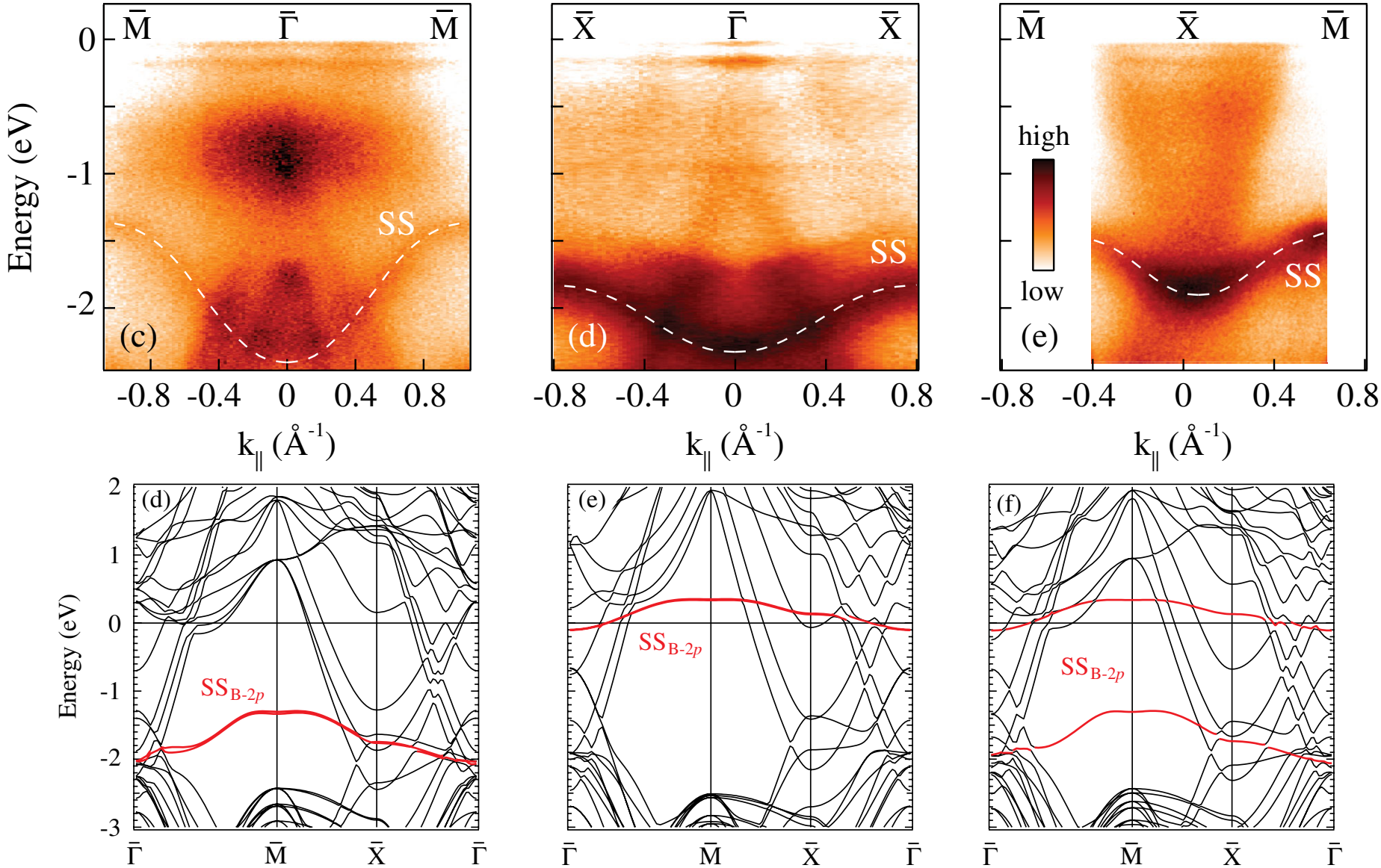

Z.-H. Zhu, et al. *Phys. Rev. Lett.* **111**, (2013)

Dielectric break down and electronic reconstruction

Electronic reconstruction is often compared to Zener's theory of the electrical breakdown of solid dielectrics.

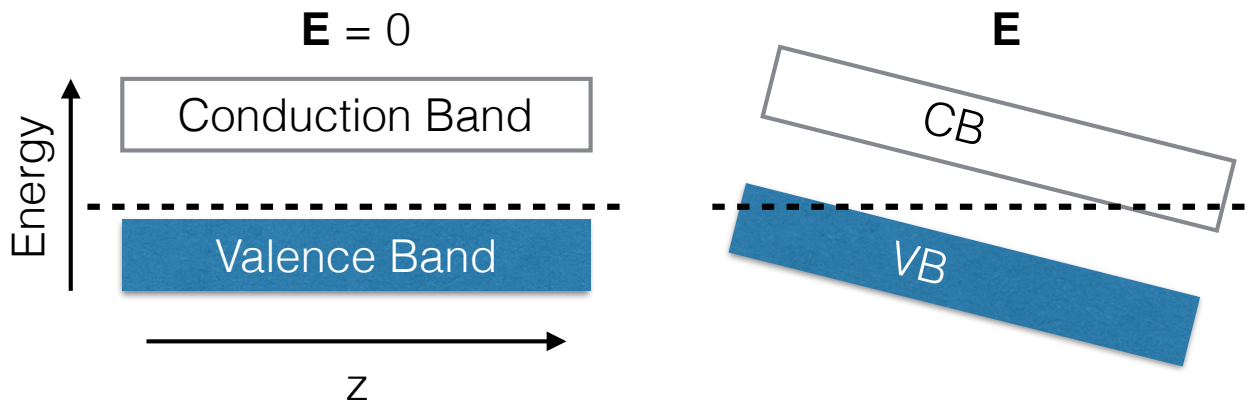

Note, some TM compounds can also compensate potential divergence by changing their valence (LaCoO3 example).

Electronic reconstructions can also be a part of complex reconstruction mechanism (Oxygen vacancies on AlO_2 surface of LAO/STO)

Simulation of various atomic geometries

Point defects

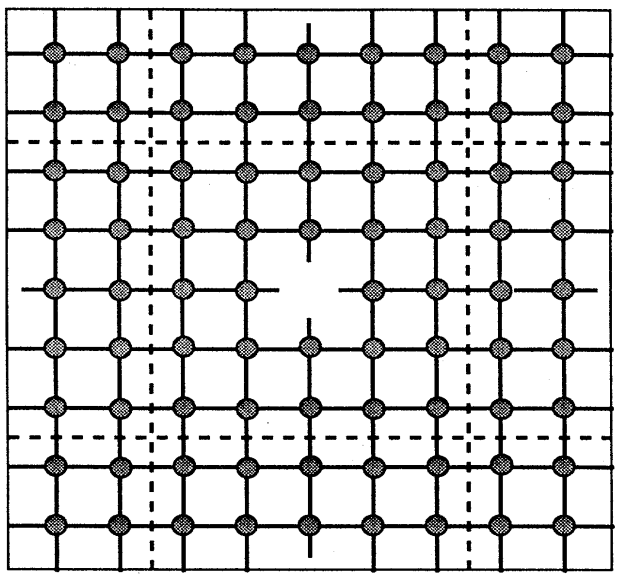

Surfaces/Interfaces

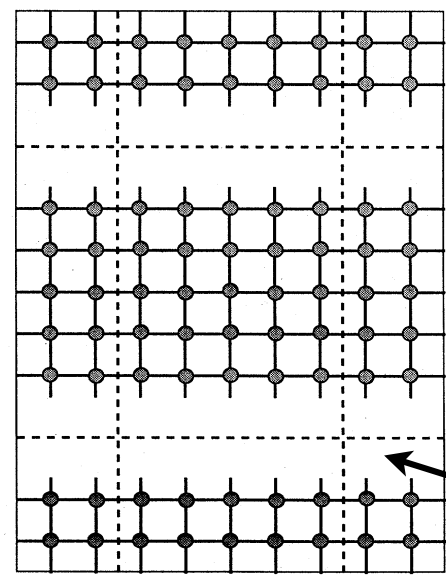

Molecules

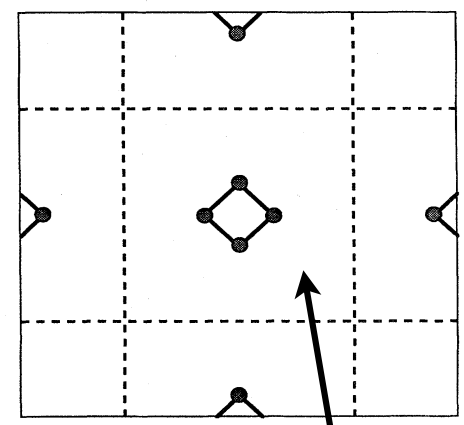

Coupling is avoided by sufficiently large vacuum region

M. C. Payne *et al*, Rev. Mod. Phys., **64**, 1045 (92)

Electronic reconstruction of MgO (111) slab

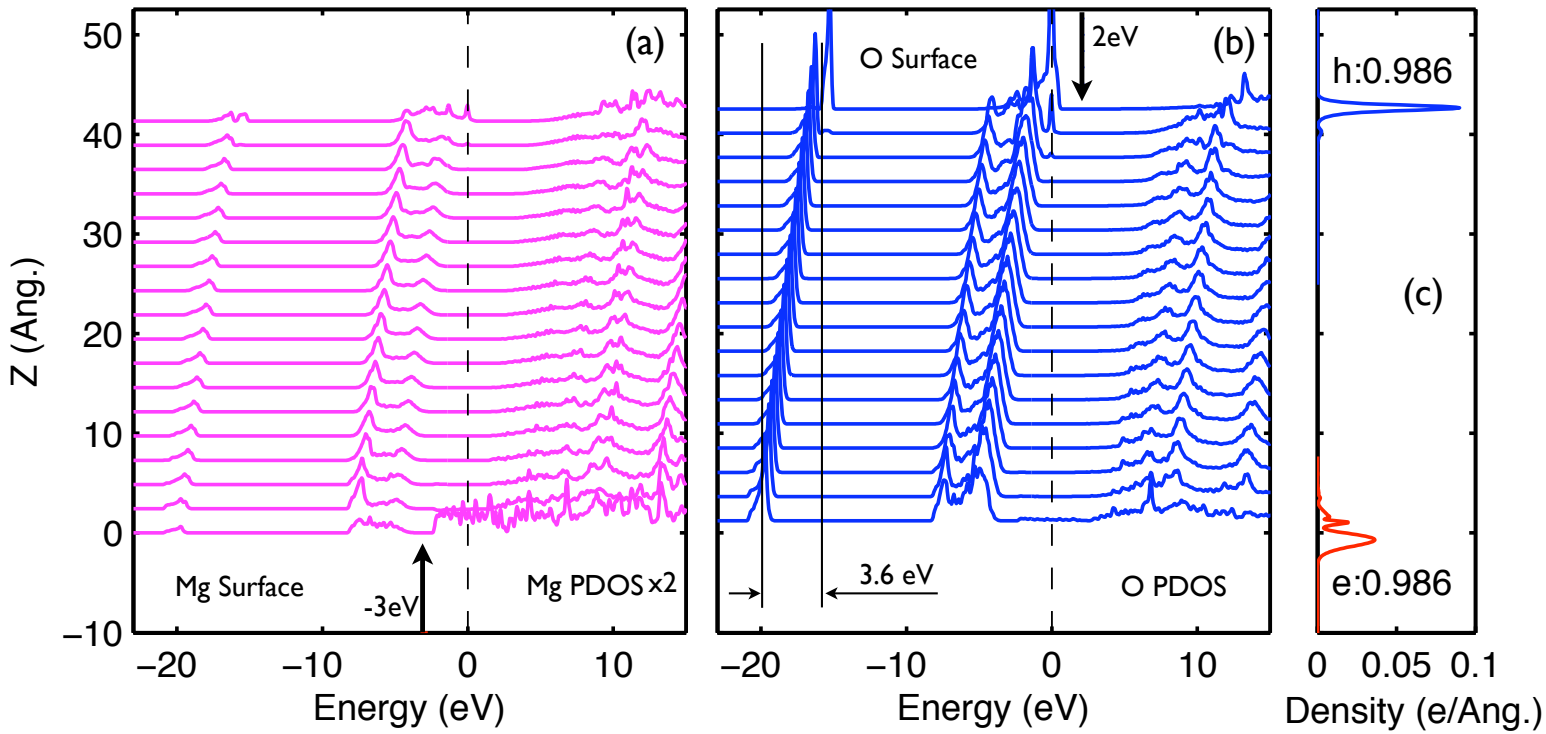

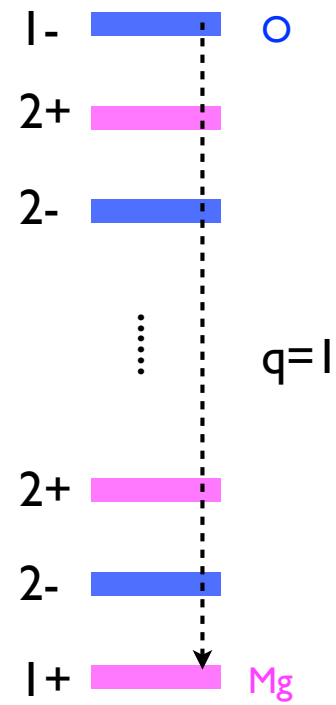

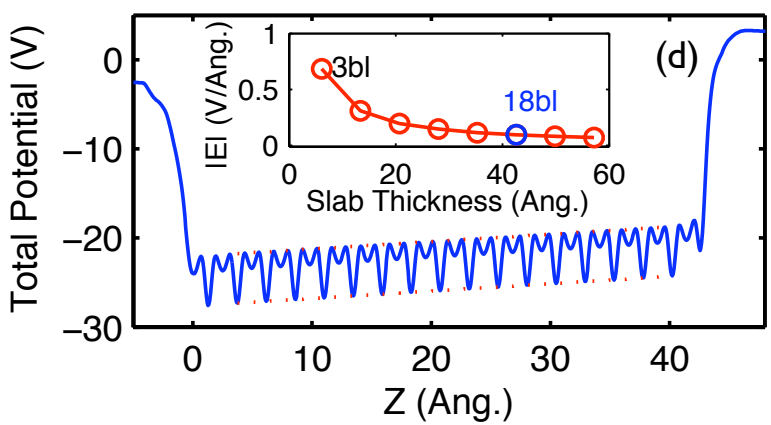

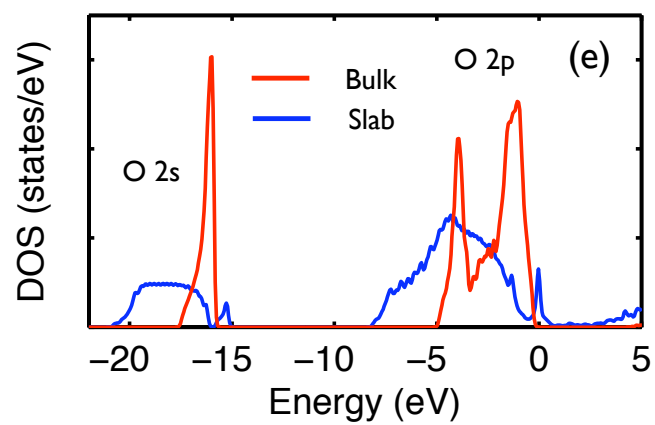

(111) surface

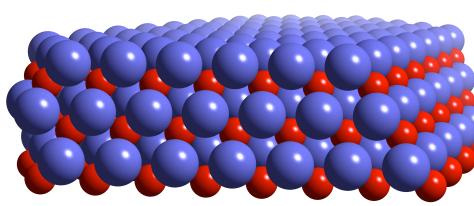

(a), (b) - GGA layer projected DOS.

(c) - Reconstructed electron and hole densities as a function of z

(d) - Planar averaged total potential as function of z

(e) - Bulk and slab total density of states. Bulk band gap is 4.5eV.

MgO-Al (111) slab: O-Al interface

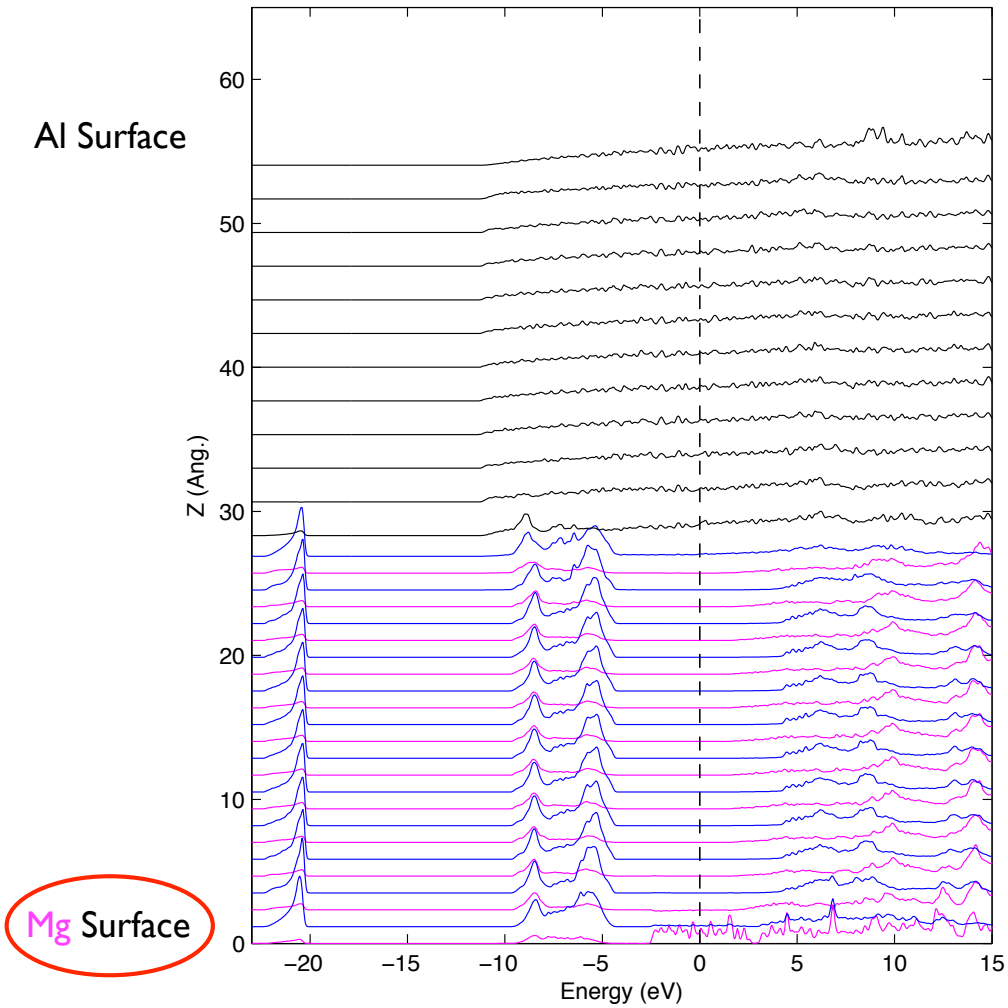

GGA layer projected DOS.

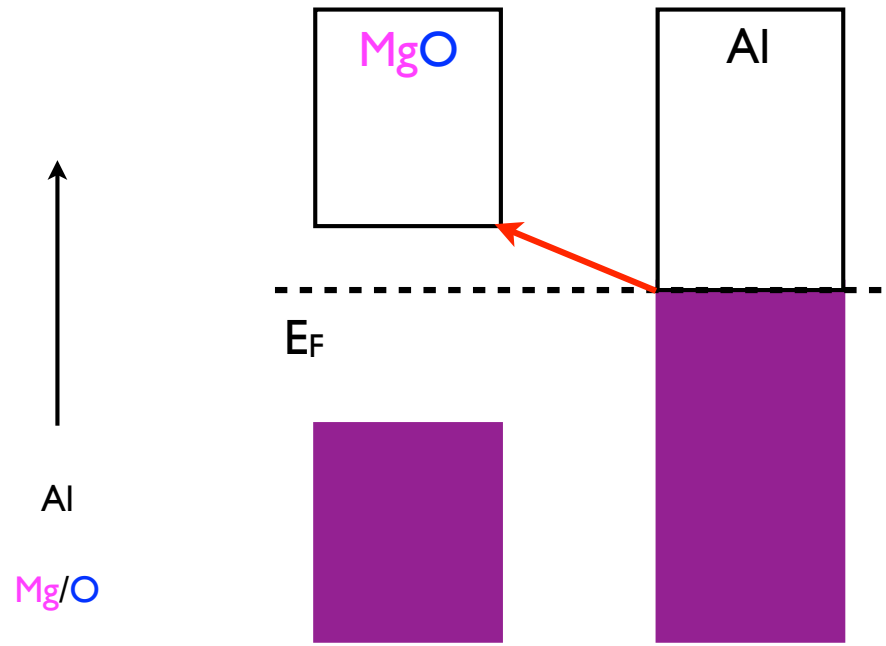

O - Al inter layer separation is 1.44A

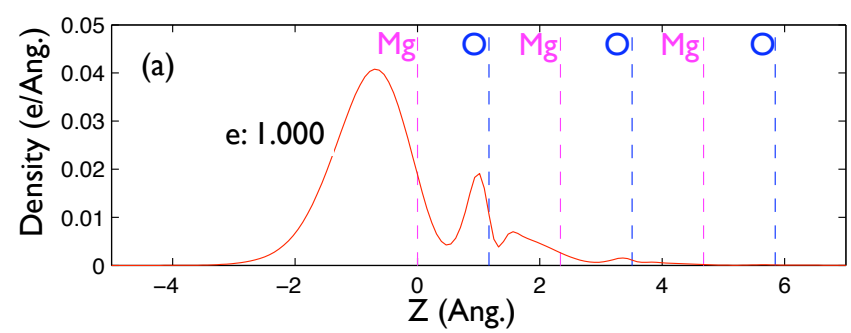

Reconstructed electron densities as a function of z in a surface region.

Relevant energy scales

- Band gaps and band alignment in semiconducting and insulating materials
- Cation and anion vacancy formation energies
- Point defect diffusion barriers
- Cohesive energy of adatoms, their ionization and electron affinity energies
- Deformation energies
- Charge transfer and d-d excitations in transition metal oxides

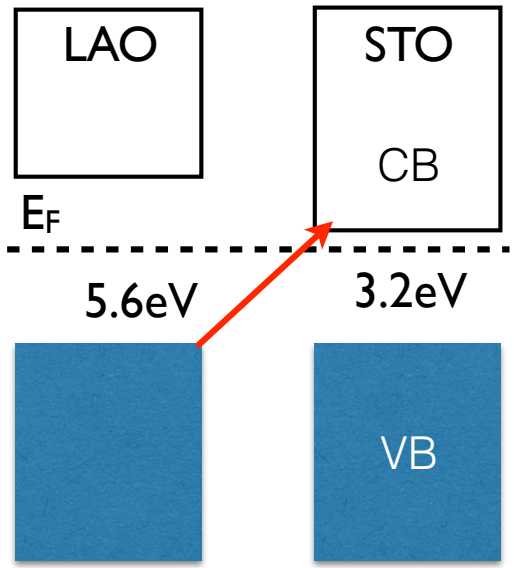

Oxygen vacancies at the LAO surface

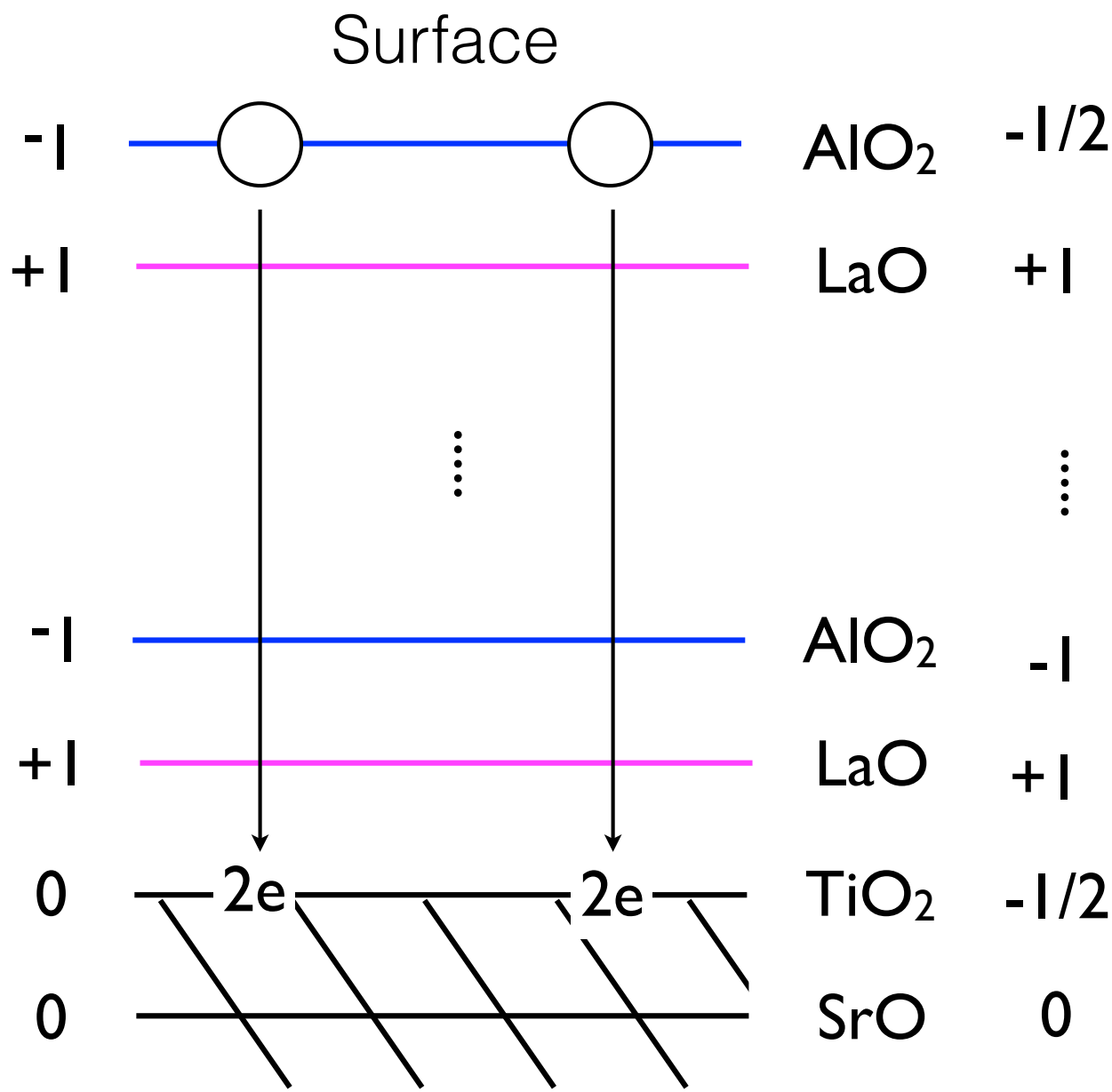

12.5% Oxygen vacancies are needed to reduce charge in surface AlO_2 layer by half.

Surface projected PDOS

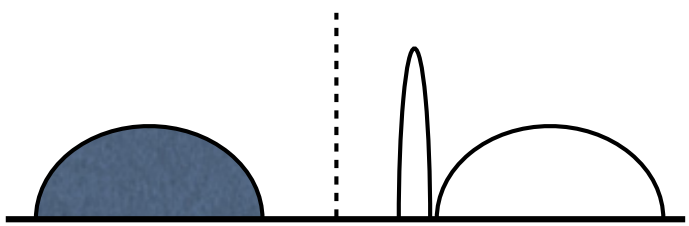

Oxygen vacancies at the LAO surface

AlO_2 surface projected DOS

TiO_2 projected DOS

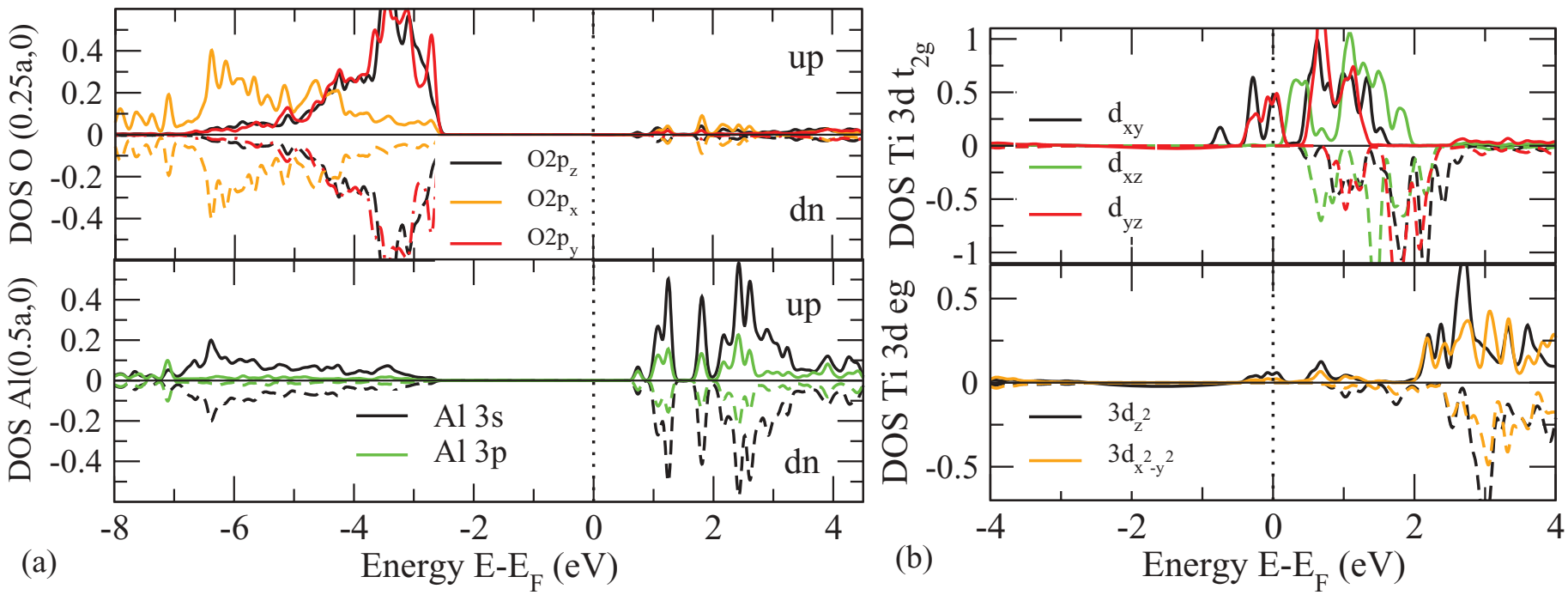

2x2x1 LaAlO3 (4uc) / SrTiO3 (1uc)

$M_{Ti}=0.56\mu_B$

Pavlenko, N., Kopp, T., Tsymbal, E., Mannhart, J. & Sawatzky, G. *Phys. Rev. B* **86**, (2012).

Oxygen formation energy in LAO/STO superlattices

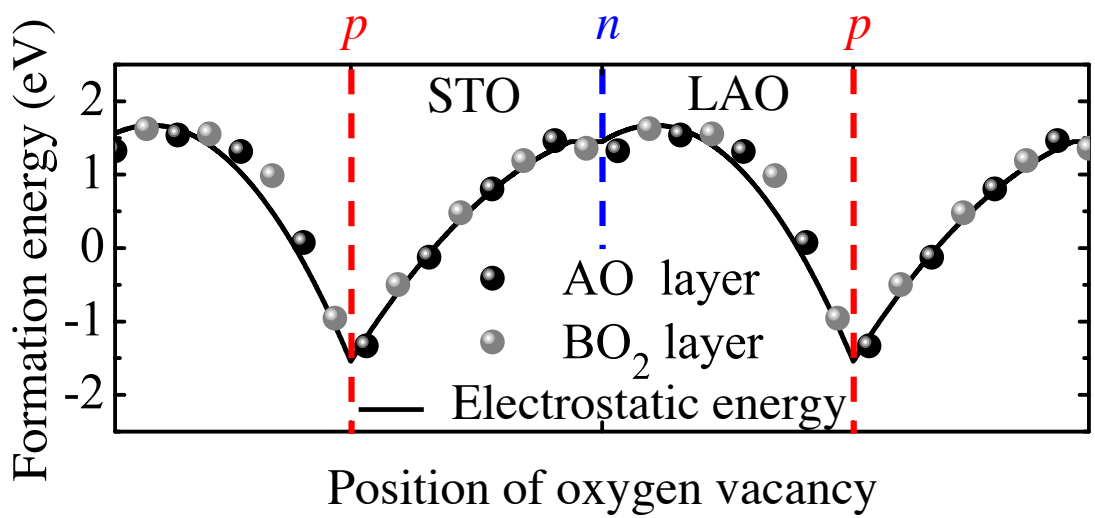

Unrelaxed lattice

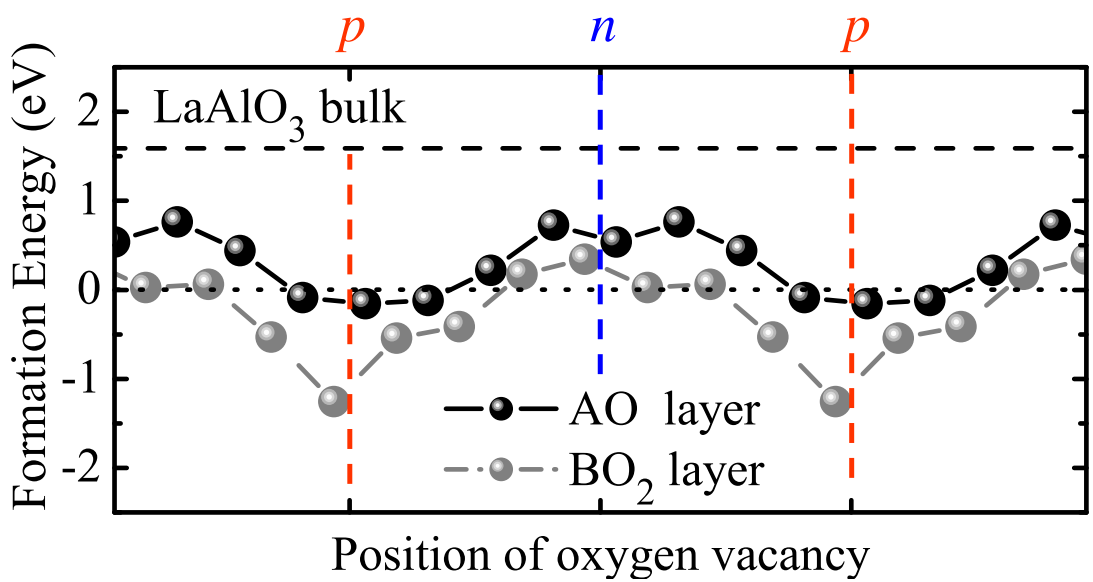

Relaxed lattice

Zhong, Z., Xu, P. X. & Kelly, P. J. *Phys. Rev. B* **82**, (2010)

Structural distortions in thin films

LAO (001)

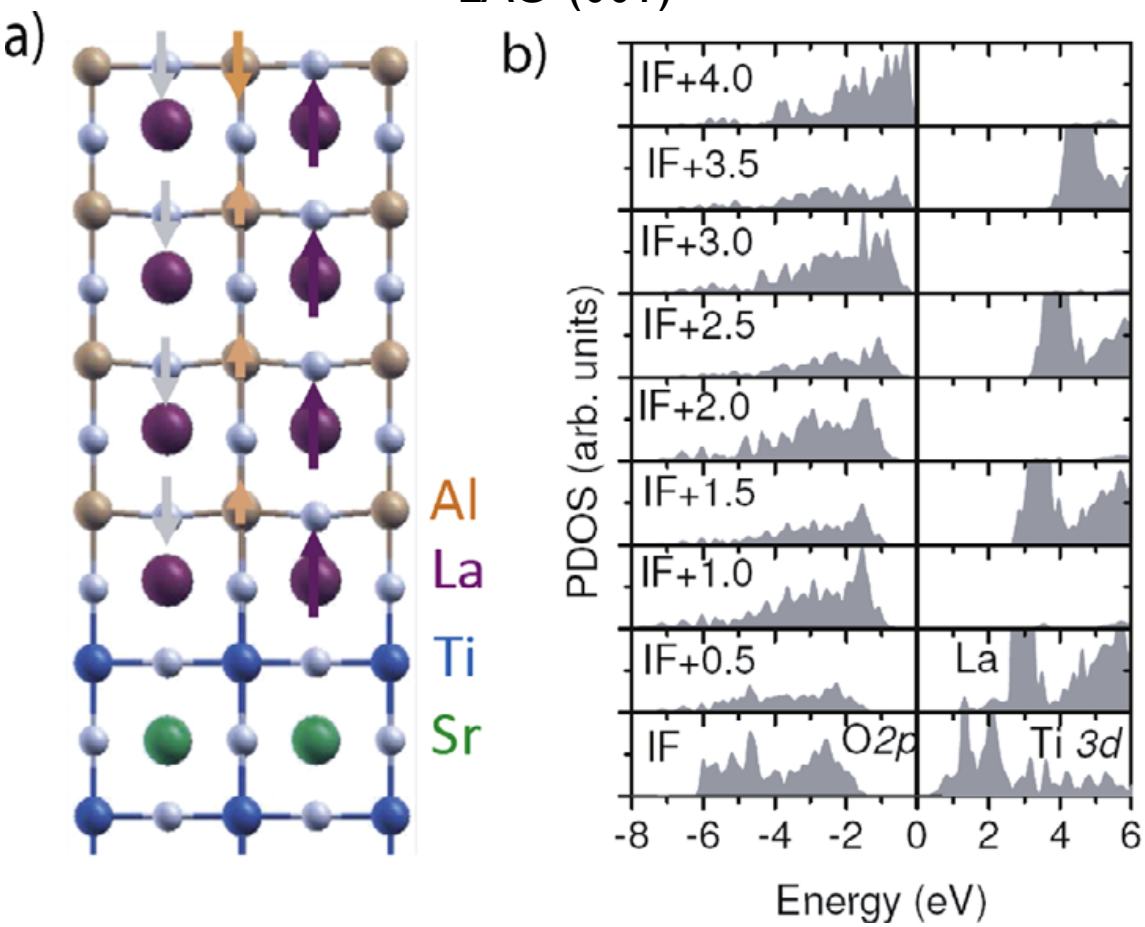

MgO (111)

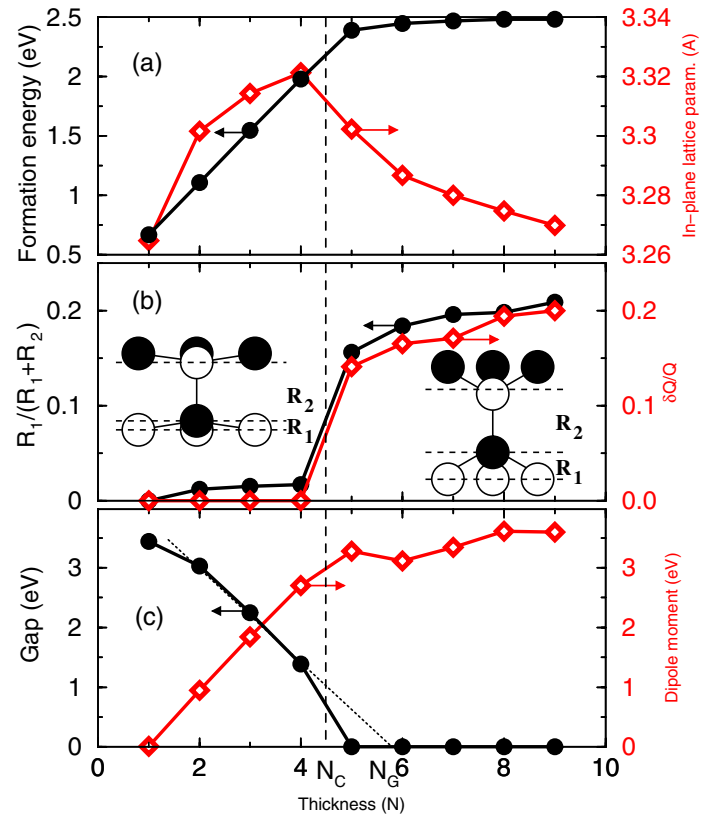

J. Goniakowski et al, PRL **98**, 205701 (2007)

Theory: R. Pentcheva and W.E. Pickett, PRL **102**, 107602 (2009)

Experiment: S.A. Pauli et al, PRL **106**, 036101 (2011)

No Oxygen vacancies on AlO_2 surface

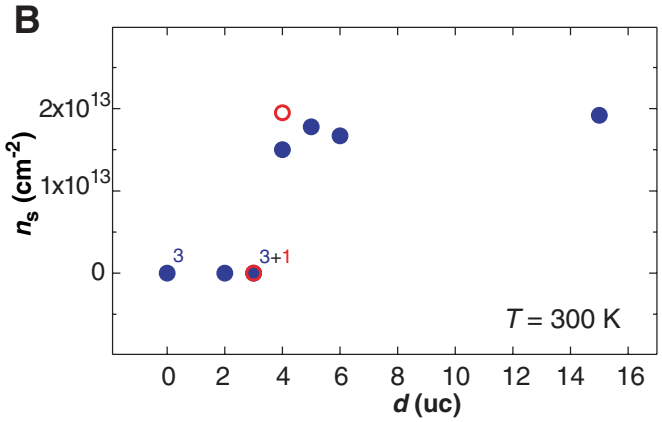

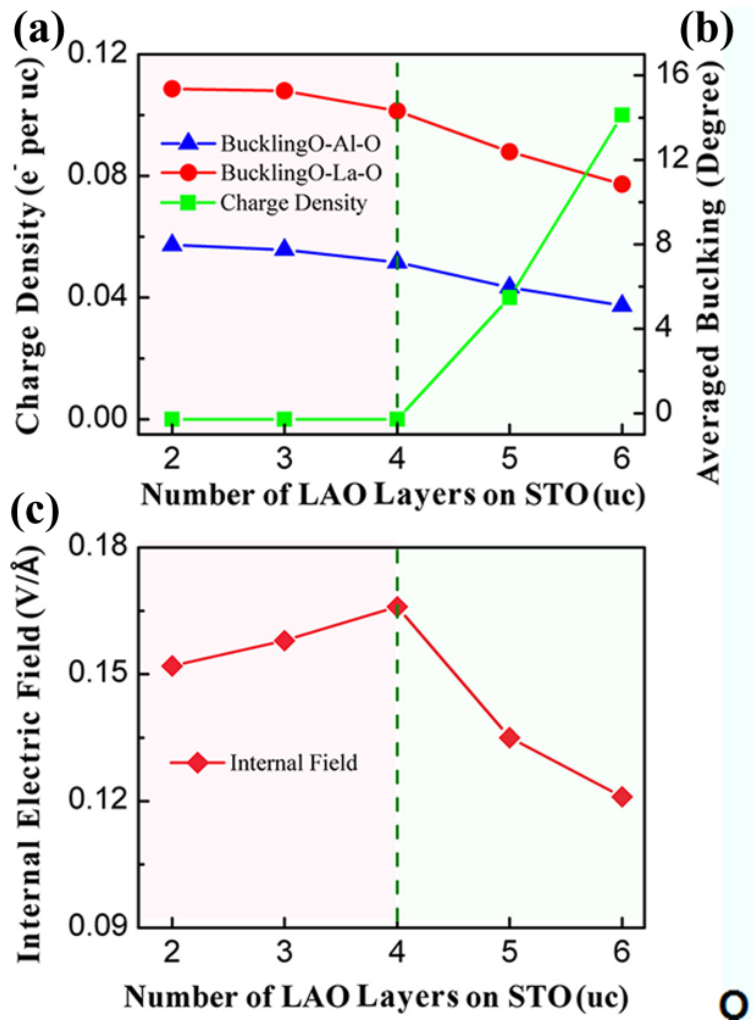

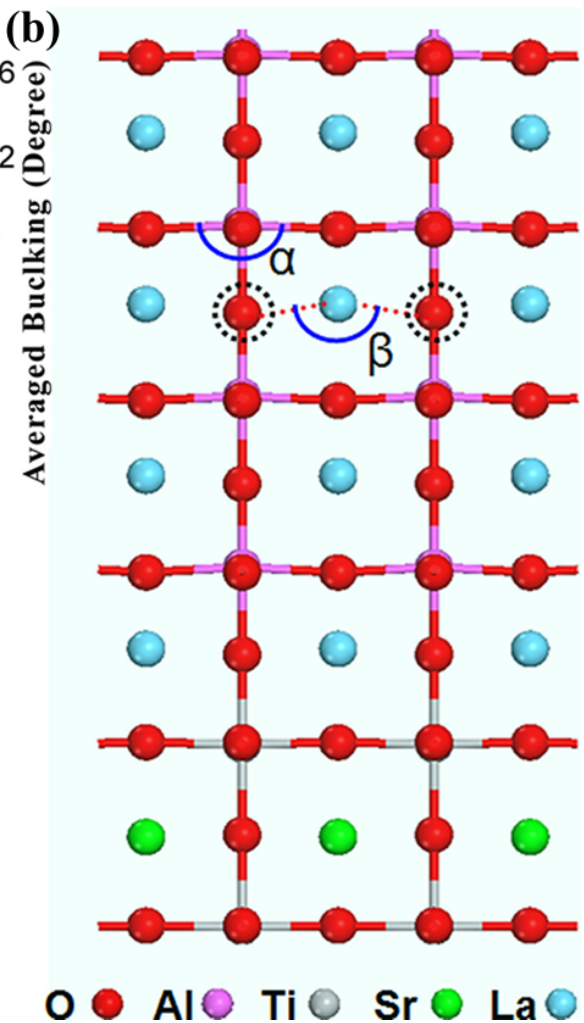

S. Thiel, et al. *Science* **313**, 1942-1945 (2006)

J. Zhou, et al, PRB 92, 125423 (2015)

Oxygen vacancies on AlO_2 surface

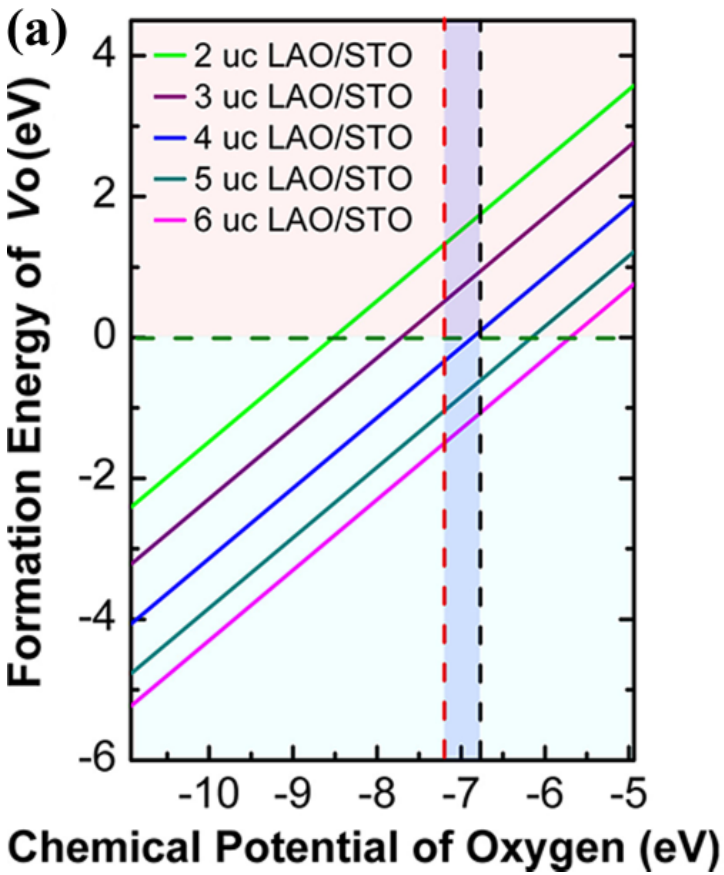

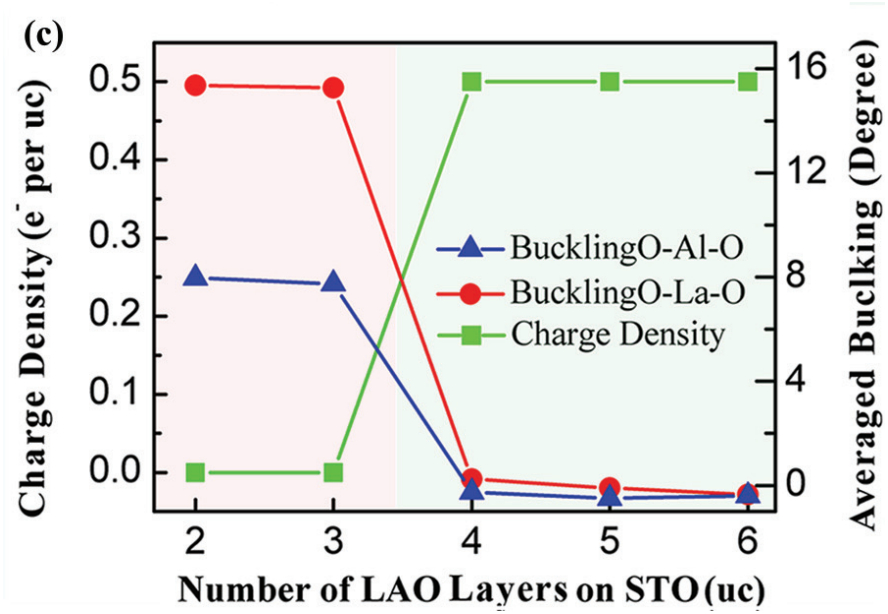

n< 4, polar distortion
n> 4, Oxygen vacancies

J. Zhou, et al, PRB 92, 125423 (2015)

Polarity induced defect mechanism

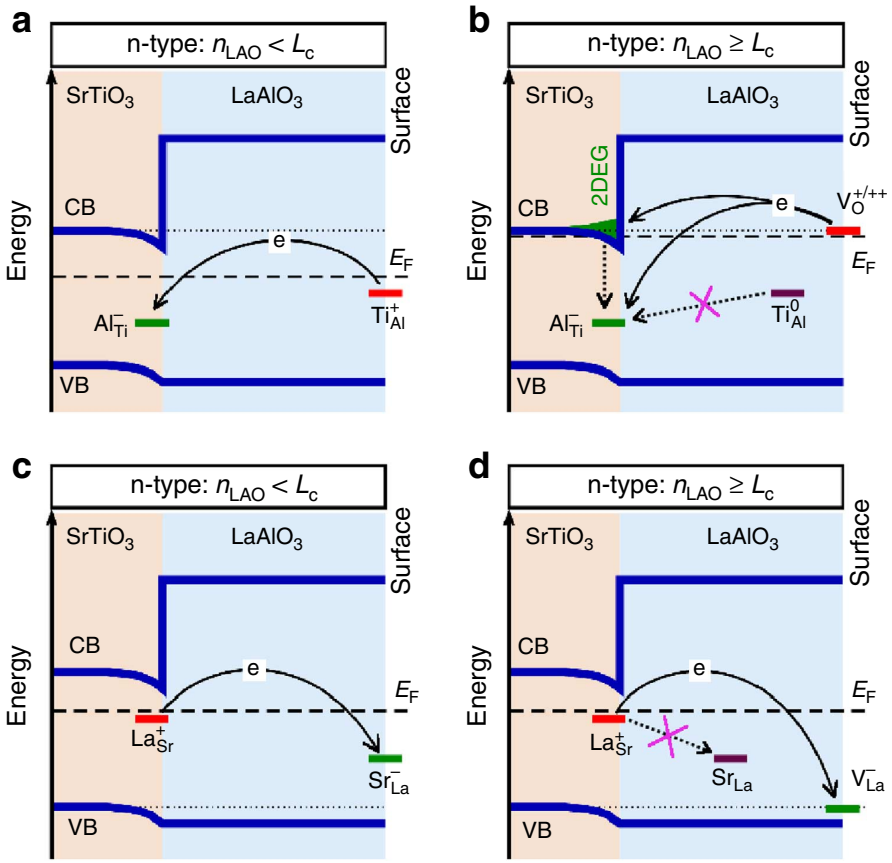

Figure 1 | Schematic band diagram and change transfer among the defects at $LaAlO_3/SrTiO_3$ interfaces. (**a**) n-type interfaces with $n_{LAO} < L_c$: all electrons transferred from $Ti_{Al}(S)$ are trapped by deep $Al_{Ti}(I)$, causing no 2DEG. (**b**) n-type interfaces with $n_{LAO} \geq L_c$: $V_O(S)$ defects donate ~ 0.5 e S_{2D}^{-1} to the interface. Part of ~ 0.5 e S_{2D}^{-1} is trapped by the $Al_{Ti}(I)$ and the rest leads to interfacial 2DEG. The formed Ti_{Al} defects are ionized, i.e., Ti^{3+}-on-Al^{3+}, having local magnetic moments. (**c**,**d**) p-type interfaces with $n_{LAO} < L_c$ (~ 4 uc) and $n_{LAO} \geq L_c$: all electrons transferred from $La_{Sr}(I)$ are trapped by $Sr_{La}(S)$ and $V_{La}(S)$, respectively. All involved defects are deep and do not induce carriers. The un-ionized Ti_{Al}^0 (not shown in **c**,**d**) also form and induce local moments. The superscripts $(0, +, ++, -)$ in the Figure denote the defect charge states, not the oxidation states of the ions there.

L. Yu and A. Zunger, *Nature Communications* **5**, 5118 (2014)

Table 2 | The specific defects and their charge transfer processes that explain the leading experimental observations at stoichiometric $LaAlO_3/SrTiO_3$ interfaces.

	n-type interface structure		p-type interface structure	
	$n_{LAO} < L_c$	$n_{LAO} \geq L_c$	$n_{LAO} < L_c$	$n_{LAO} \geq L_c$
Polar field compensation	$Ti_{Al}(S) \rightarrow Al_{Ti}(I)$	$V_O(S) \rightarrow Al_{Ti}(I)$ and $V_O(S) \rightarrow$ CBM(I)	$La_{Sr}(I) \rightarrow Sr_{La}(S)$	$La_{Sr}(I) \rightarrow V_{La}(S)$
Origin of 2DEG/2DHG	No 2DEG: $Al_{Ti}(I)$ traps all electrons from $Ti_{Al}(S)$	$V_O(S) \rightarrow$ CBM(I): $Al_{Ti}(I)$ traps part of electrons from $V_O(S)$	No 2DHG: $La_{Sr}(I)$ traps all holes from $Sr_{La}(S)$	No 2DHG: $La_{Sr}(I)$ traps all holes from $V_{La}(S)$
Density of 2DEG/2DHG	Zero	< 0.5 e S_{2D}^{-1}	Zero	Zero
Origin of critical thickness	Polar-field induced $V_O(S)$ formation		Polar-field induced $V_{La}(S)$ formation	
Origin of interface magnetism	Ti^{4+}-on-Al^{3+} forms but has no local moment	Ti^{3+}-on-Al^{3+} forms and induces local moment	Ti^{3+}-on-Al^{3+} forms and induces local moment	Ti^{3+}-on-Al^{3+} forms and induces local moment

The "S" and "I" denote the $LaAlO_3$ free surface and $LaAlO_3/SrTiO_3$ interface, respectively. S_{2D} is the two-dimensional unit cell area.

Electropositive cations as surfactants

Motivation:

- defect free films, heterostructures, etc
- (111) terminated MnS stabilized by adsorption of I^- [a]
- Bi is used to increase surface smoothness and enhance N incorporation in GaN_xAs_{1-x} [b]
- K is used to electron doped YBCO [c]

(a) H. H. Heikens, et al, Jpn. J. Appl. Phys. 19, 399 (1980).
(b) S. Tixier, et al, J. Cryst. Growth 251, 449 (2003); E. Young, et al, J. Cryst. Growth 279, 316 (2005).
(c) D. Fournier, et al, Nature Phys. 6, 905 (2010); M. A. Hossain, et al, Nature Phys. 4, 527 (2008)

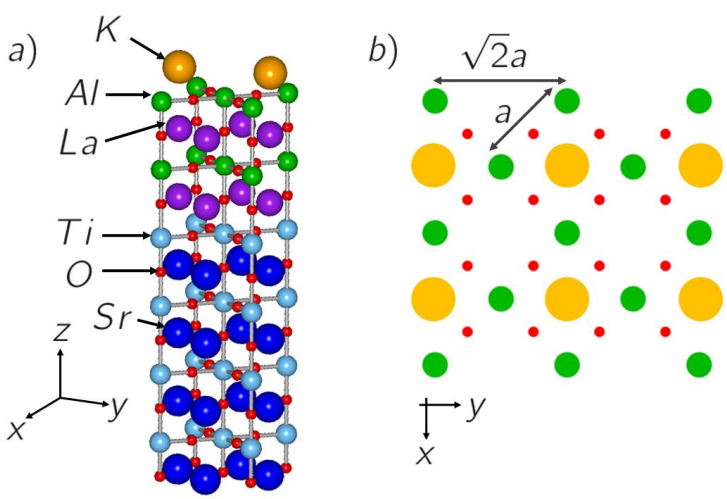

Test system:

$LaAlO_3$ films on $SrTiO_3$ substrate

Electropositive cations as surfactants

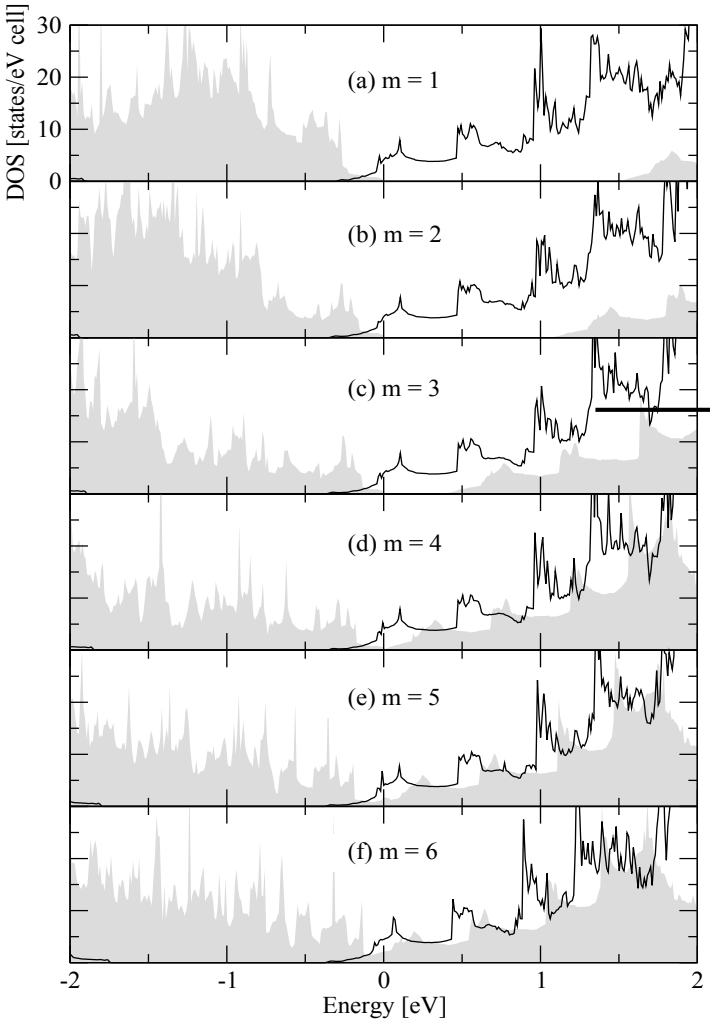

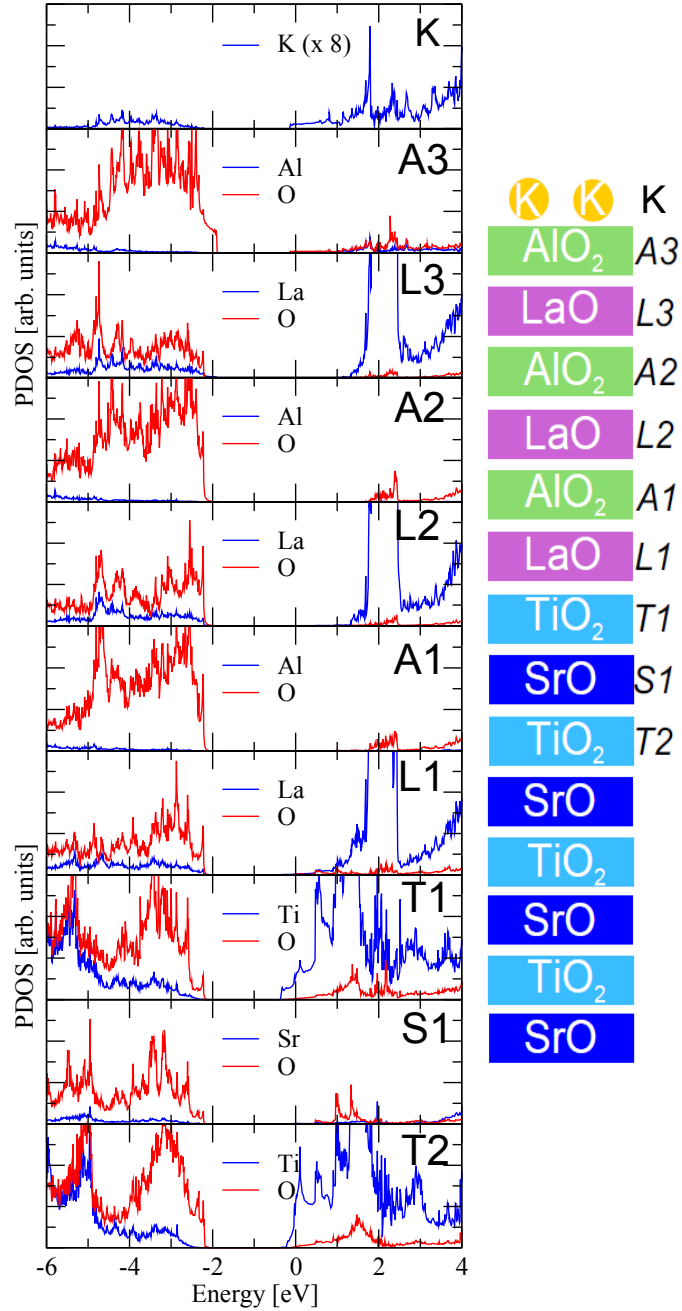

FIG. 3. Total DOS for $(LAO)_m(STO)_4$, $m = 1 - 6$, with (black line) and without (shaded gray) K adsorption. The Fermi energy is at 0. The scale is the same for all panels. The critical thickness at which the system without K undergoes electronic reconstruction and becomes conducting is 4 unit layers of LAO. In contrast, the system with K is conducting at all LAO thicknesses simulated.

Electropositive cations as surfactants

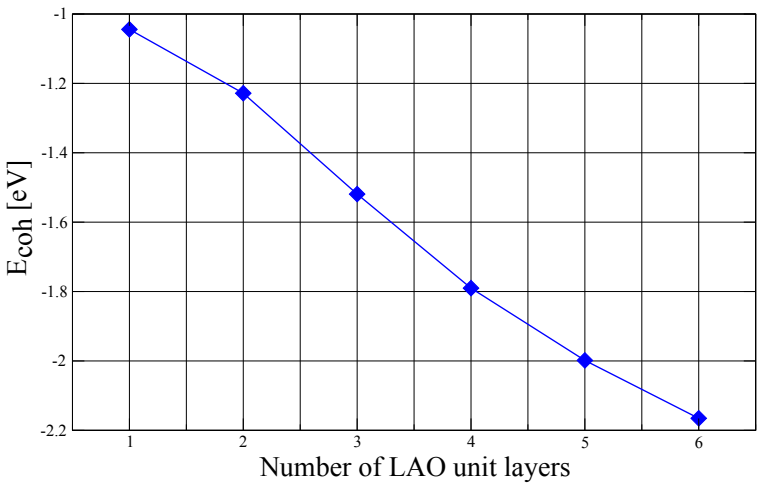

FIG. 4. (Color online) Cohesive energy per adsorbed K, defined in Eq. (1), as a function of the thickness of LAO. The system with adsorbed K becomes more stable as the thickness increases. The cohesive energy is approximately 1 eV for 1 unit layer of LAO, increasing to over 2 eV as the LAO thickness is increased.

$$E_{coh}(m) = E_{K_{ads}LAO_mSTO_4} - E_{LAO_mSTO_4} - E_K$$

Ecoh increases after 50% by 0.8eV per K

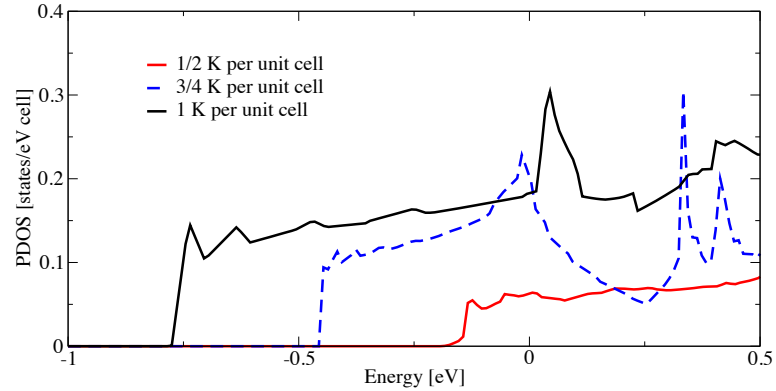

FIG. 5. (Color online) K PDOS near the Fermi energy ($E = 0$), at three cases of K coverage, for LAO thickness of two unit layers. The density of conduction electrons retained by K increases significantly going from 1/2 to 3/4 per unit cell coverage, and then from 3/4 to 1 per unit cell coverage. Hence, K adsorption beyond the critical amount needed for the ideal exact compensation does not result in extra electrons being transferred to the interface; the extra electrons remain in the K overlayer.